

Published in final edited form as:

J Am Soc Mass Spectrom. 2014 March ; 25(3): 398–409. doi:10.1007/s13361-013-0785-8.

The Role of Methoxy Group in the Nazarov Cyclization of 1,5-bis-(2-Methoxyphenyl)-1,4-Pentadien-3-one in the Gas Phase and Condensed Phase

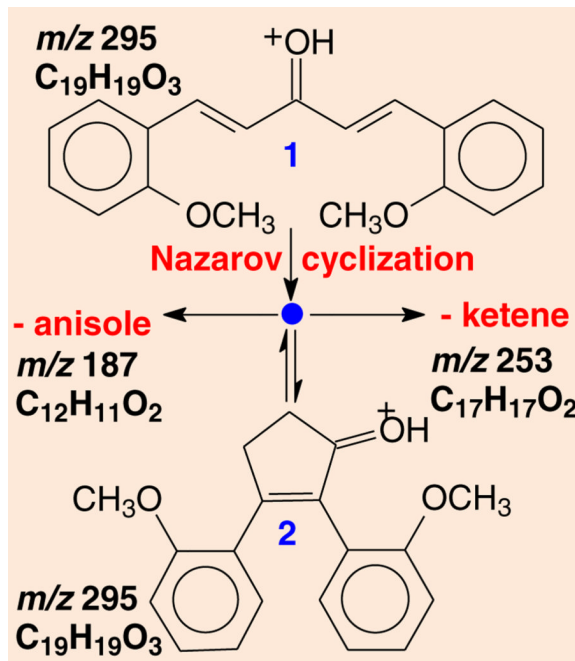
June Cyriac¹, Justin Paulose¹, Mathai George¹, Marupaka Ramesh², Ragampeta Srinivas², Daryl Giblin³, and Michael L. Gross³

¹Department of Chemistry, Sacred Heart College, Thevara, Cochin, Kerala, India

²National Center for Mass Spectrometry, IICT, Hyderabad, India

³Department of Chemistry, Washington University in St. Louis, St. Louis, MO 63130, USA

Abstract



ESI-protonated 1,5-bis-(2-methoxyphenyl)-1,4-pentadien-3-one (1) undergoes a gas-phase Nazarov cyclization and dissociates via expulsions of ketene and anisole. The dissociations of the $[M+D]^+$ ions are accompanied by limited HD scrambling that supports the proposed cyclization. Solution cyclization of 1 was effected to yield the cyclic ketone, 2,3-bis-(2-methoxyphenyl)-cyclopent-2-ene-1-one, (2) on a time scale that is significantly shorter than the time for cyclization of dibenzalacetone. The dissociation characteristics of the ESI-generated $[M + H]^+$ ion of the synthetic cyclic ketone closely resemble those of 1, suggesting that gas-phase and solution

cyclization products are the same. Additional mechanistic studies by density functional theory (DFT) methods of the gas-phase reaction reveals that the initial cyclization is followed by two sequential 1,2-aryl migrations that account for the observed structure of the cyclic product in the gas phase and solution. Furthermore, the DFT calculations show that the methoxy group serves as a catalyst for the proton migrations necessary for both cyclization and fragmentation after aryl migration. An isomer formed by moving the 2-methoxy to the 4-position requires relatively higher collision energy for the elimination of anisole, as is consistent with DFT calculations. Replacement of the 2-methoxy group with an OH shows that the cyclization followed by aryl migration and elimination of phenol occurs from the $[M + H]^+$ ion at low energy similar to that for 1.

Keywords

Ion chemistry; Density functional theory; Nazarov cyclization; Solution and gas phase; Analogies; Electrospray ionization; Tandem mass spectrometry

Introduction

One of the methods of choice for the synthesis of substituted cyclopentenones is the acid-catalyzed, electrocyclic ring closure of divinyl ketones, a reaction known as the Nazarov cyclization [1, 2] and one for which the effects of substituents and transition metal catalysts have been explored [3]. The proposed mechanism involves a conrotatory ring closure of the protonated divinyl ketone followed by hydrogen migrations to yield the product [3], Scheme 1, first part. The reaction is a useful synthesis tool for synthesis of compounds including natural products [4], heterocycles [5], and chiral molecules [6]. Molecular orbital calculations indicate that various substituents at the third carbon relative to the carbonyl group of the divinyl ketone affect the activation energy required for cyclization [7]. The reaction mechanism of cyclization and the effect of acids on the activation energy for cyclization were also explored by molecular orbital calculations using DFT methods [8]. Molecular orbital calculations have established the catalytic role of a water molecule in the hydrogen rearrangements involved in the metal-mediated Nazarov cyclization [9]. The catalytic role of other solvents (e.g., methanol [10] and acetonitrile [11]) are known in effecting symmetry-forbidden 1,3-hydrogen migrations in acetone radical cations, as demonstrated by mass spectrometry (MS) and supported by molecular orbital calculations.

The utility of MS for the study of gas-phase reactions [12] and their relationship to condensed phase reactions is now well established, a classic example being the gas-phase Claisen rearrangement of allyl phenyl ether as ionized by chemical ionization [13]. Electrospray ionization (ESI) also facilitates production of protonated or deprotonated molecules in the ion source of a mass spectrometer and their introduction into the gas phase for studies by tandem MS. Combining the results with those from DFT calculations provides a useful approach in exploring reaction mechanisms, especially for protonated or deprotonated molecules. Examples are the investigation of mechanisms of the rearrangement of protonated 2-nitophenylphenyl ethers [14, 15] and that of the Smiles rearrangement [16, 17].

The acid-catalyzed (formic and phosphoric acid 1:1) cyclization of protonated dibenzalacetone (**i**) (1,5-diphenyl-1,4-pentadien-3-one) occurs at 90 °C in 28 h to give a cyclopentenone in moderate yield. The structure of the product, characterized as 2,3-diphenylcyclopent-2-ene-1-one (**iii**), appears to have changed the position of the carbonyl group, and a tentative reaction scheme was proposed (Scheme 1) [18]. The mechanism of product formation may be that the initially formed enol (**ii**) of the cyclopenteneone

isomerizes via a 1,2-shift of the OH group, in acid medium, to yield the enol form of the product, which then tautomerizes to the keto form (**iii**). Recent studies on Nazarov cyclizations revealed that under certain conditions, 1,2-shifts of groups such as phenyl or alkyl occur after the cyclizations, a process utilized for the synthesis of spiro-compounds [19].

Recently, we investigated the gas-phase Nazarov cyclization of protonated 2-methoxychalcone by using tandem MS and DFT calculations [20]. We concluded that the gas-phase cyclization is analogous to its solution-phase process; the latter is promoted by microwave irradiation in trifluoroacetic acid [21]. Moreover, we demonstrated that the methoxy group serves as an effective catalyst for proton transfers involved in completion of the gas-phase cyclization and subsequent rearrangement and dissociation. Encouraged by those results, we designed an ESI tandem MS study of 1,5-bis-(2-methoxyphenyl)-1,4-pentadien-3-one (**1**) to investigate whether the Nazarov cyclization occurs upon protonation of this molecule. We again employed DFT methods to understand the catalytic role that the methoxy group plays in facilitating the reaction and subsequent fragmentations. Furthermore, we determined by DFT calculations the role that phenyl or hydroxyl migration plays after the ring closure leading to the observed cyclization product. To further delimit the roles the methoxy group plays in the gas-phase cyclization, we also investigated the fragmentations of protonated 1,5-bis-(4-methoxyphenyl)-1,4-pentadien-3-one (**3**), dibenzalacetone (**4**), and 1,5-bis-(2-hydroxyphenyl)-1,4-pentadien-3-one (**5**, Scheme 2). The 2,3-bis-(2-methoxyphenyl)-cyclopent-2-ene-1-one (**2**) was synthesized by cyclization of **1** in a mixture (1:1) of formic acid and phosphoric acid at 80 °C to afford a reference compound for testing for the cyclization in the gas phase.

Experimental

Synthesis

The dibenzalacetones **1**, **3**, **4**, and **5** used for the experiments were prepared from acetone and the appropriate benzaldehyde by following literature procedures [22–24]. The substituted cyclopentenone **2** was obtained by the cyclization of **1** following a previously reported procedure [18] for the cyclization of **4**, but the temperature used for the experiment was only 80 °C and the reaction was essentially complete in 5 h as determined by TLC analysis. The reaction mixture was diluted with water, and the product was extracted with ethyl acetate and purified by silica gel column chromatography, using a mixture of petroleum ether and ethyl acetate. A comparison of the ¹H NMR spectra of **1**, **3**, **4**, and **5** with those previously reported [23] confirmed that the structures were correct. The ¹H NMR spectrum of **2** showed the following signals: δ 7.18–7.20 (2H, m), 6.99–7.18 (2H, m), 6.70–6.90 (4H, m), 3.55 (3H, s), 3.68, (3H, s), 3.1 (2H, m), 2.70 (2H, m).

Mass Spectrometry

The protonated molecules were introduced into the gas phase by using ESI of a solution of the compounds in 1:1 mixture of H₂O/acetonitrile by direct infusion (flow rate: 5 μL/min). The dissociation pathways of the [M + H]⁺ ions were first explored by ESI MS and collisionally activated dissociation experiments (MS/MS and MS³) were initially performed by using the Thermo LCQ Deca Ion-Trap (San Jose, CA, USA) mass spectrometer operated in the positive-ion mode at low mass resolving power. To determine the elemental compositions of the precursor ions and fragment ions, the ESI MS and ESI-CAD experiments were repeated at a mass resolving power of 30,000 by using the Thermo LTQ-Orbitrap mass spectrometer operated in the positive-ion mode. The source parameters were optimized to get maximum sensitivity. The needle voltage was 3 kV, and cone voltage was 90 V. Dry nitrogen gas at 150 °C was used to desolvate the ions. The collision energies were

set to a minimum value required to make the abundance of the most abundant fragment exceed that of the precursor ion (between 16 % and 30 % of the available energy). To aid in elucidation of the rearrangement processes, $[M + D]^+$ ions were produced in the gas phase by ESI from solutions of the compounds in 1:1 D_2O /acetonitrile mixture by direct infusion, and CAD spectra were recorded at low mass resolving power.

Theoretical Calculations

To characterize the potential energy surface (PES) associated with fragmentation, we performed theoretical calculations. Conformer spaces for precursors and intermediates were explored by Monte-Carlo/MMFF molecular mechanics/dynamics methods. From these results, structures of precursors, intermediates, and scans for associated transition states were explored by using the PM3 semi-empirical [25, 26] algorithm (Spartan for Linux; Wavefunction, Inc., Irvine, CA), and if necessary, scans were also performed by DFT: B3LYP/6-31G(d,p). The possible minima and transition states so obtained were geometrically optimized by DFT (Density Functional Theory, part of Gaussian 98/03/09 suites [27–29], by Gaussian Inc., running on various computer systems) to level B3LYP/6-31G(d,p) and confirmed by vibrational frequency analysis (geometries in Supplementary Data, Table 5). Connections of transition states to minima were examined by inspection, projections along normal reaction coordinates, and path calculations as necessary. Final single-point energies were calculated at level M06/6-311+G(2d,p), which employed the M06 hybrid functional with good general accuracy [30, 31], on the B3LYP/6-31G(d,p) geometries to which scaled thermal-energy corrections were applied [32] and reported in Tables 2, 3, 4. DFT was selected for high-level calculations because it requires less computational overhead than ab initio methods and performs adequately [33]. In addition for comparison purposes, single-point energies were calculated at levels B3LYP/6-311+G(2d,p) and MP2(fc)/6-311+G(2d,p) on the B3LYP/6-31G(d,p) geometries, with the results being averaged [34] to which scaled thermal-energy corrections were applied. The differences and their sum as an RMS deviation are reported in kJ/mol (Supplementary Data, Tables S1–S4). All results are reported in kJ/mol as enthalpies of formation relative to a selected, suitable precursor designated as **A₁** for all precursors that have conformations suitable for Nazarov cyclization.

Results and Discussion

Empirical Results

Protonated 1,5-bis-(4-methoxyphenyl)-1,4-pentadien-3-one, as the $[M + H]^+$ generated by electrospray ionization of our synthetic sample, yields fragment ions of m/z 253 and 187 by the eliminations of the elements of ketene and anisole, as evidenced by its CAD mass spectrum. CAD at high mass resolving power (Figure 1a) afforded the molecular formula of the fragment ions and confirmed the proposed eliminations (Table 1). To determine the course of the rearrangement processes, the corresponding $[M + D]^+$ ions were investigated by CAD. The $[M + D]^+$ ions dissociate via eliminations of ketene and ketene-d, to yield fragment ions of m/z 254 and 253 in the ratio 2:1, and of anisole and anisole-d to generate fragment ions of m/z 188 and 187 in the ratio 2.5:1, as revealed by the CAD mass spectrum. The elimination of ketene and anisole together with the occurrence of HD scrambling in the course of fragmentation of the $[M + D]^+$ ions of **1** indicate some rearrangement/scrambling processes of the protonated molecule upon CAD. Given that Compound **1** is a divinyl ketone, a gas-phase Nazarov cyclization is likely for the $[M+H]^+$ ions of **1**; hence, we proposed that the observed fragmentation results from an intermediate initially formed by Nazarov cyclization, (Scheme 3). Further, it was initially envisaged that the intermediate **a**, formed by the cyclization, rearranges to **b** owing to the abstraction of the proton from carbon-3 by the methoxy group. Subsequent hydrogen migrations in ion **b** mediated by the

methoxy group are necessary for the formation of the fragment ions, a hypothesis explored further by molecular orbital calculations.

The most appropriate reference compound for establishing the gas-phase cyclization of Compound **1** would be the neutral ketone corresponding to the cyclic intermediate **b**. To prepare this reference compound, the cyclization of **1** was conducted by heating the precursor in solution in a 1:1 mixture of formic and phosphoric acids at 80 °C. The reaction, essentially complete in 5 h, yields the product, 2,3-bis-(2-methoxyphenyl)-cyclopent-2-ene-1-one (**2**). This product does not have structure of **b** in Scheme 3 but an isomer (Scheme 4). The results show that the Nazarov reaction does occur at a lower temperature and shorter time when the methoxy group is present at the 2-position of dibenzalacetone than for the unsubstituted compound. The structures of the products from both compounds, however, have the same relative positions of the phenyl groups with respect to the carbonyl group [18].

The ESI positive-ion CAD spectrum of **2** is closely similar to that of **1**, and the molecular ions of both compounds dissociate by the same set of fragmentations (Figure 1b). The elemental compositions of each of the fragment ions are identical from both precursors as revealed by the measured accurate masses (Table 1). Moreover, MS³ experiments show that the dissociations of the major fragment ions of *m/z* 253 and 187 originating from Compounds **1** and **2** are closely similar. Moreover, CAD also demonstrates that the [M + D]⁺ ion of **2** dissociates by the expulsion of ketene without HD scrambling into the ketene to yield a fragment ion of *m/z* 254, whereas the elimination of anisole from the [M + D]⁺ ion involves HD scrambling so that peaks corresponding to fragment ions of *m/z* 188 and 187 (1:1) are observed. By comparison, the elimination of ketene from the [M+D]⁺ ion of **1** indicates HD scrambling involving at least 2H. The elimination of ketene from protonated **2**, likely generated from the carbonyl and adjacent methylene, must involve no HD scrambling between the methylene and the charging protons; the latter must be transferred elsewhere. The expulsion of anisole appears to involve HD scrambling of the carbonyl proton/deuteron with the equivalent of one other proton. The similarities in the dissociation pattern of **1** and **2** suggest that ESI protonation of **1** induces it to rearrange to protonated **2** via Nazarov cyclization followed by shift of either the hydroxyl or aryl groups. Fragmentations of both compounds likely occur via a common intermediate, resulting in identical fragmentations (Scheme 5).

The CAD mass spectrum of the ESI-generated [M + H]⁺ of **3** shows *m/z* 187 and 253 fragment ions by expulsions of anisole and ketene, respectively. The molecular formulae of the fragment ions given in Table 1 also support the proposed eliminations of anisole and ketene. The collision energy, however, needed to obtain a mass spectrum with similar abundances for the ion of *m/z* 187 (90 % of the precursor ion) (Figure 2a) is greater than that for Compound **1**. Thus, the Nazarov cyclization and subsequent eliminations of anisole and ketene also appear to occur for the 4-methoxy compound, **3**, but the CAD requires higher energy than for **1** and **2** and must necessarily involve different pathways. In addition, the elimination of anisole from the [M + D]⁺ ion of **3** occurs with HD scrambling to yield fragment ions of *m/z* 188 and 187 in the ratio 0.8:1, compared with 1:1 for **1** and **2**. In contrast, the elimination of ketene occurs with HD scrambling to yield fragment ions of *m/z* 254 and 253 in the ratio 4:1, whereas for **1** and **2** there is no HD scrambling. Moreover, the ESI generated [M + H]⁺ of *m/z* 235 of dibenzalacetone, **4**, dissociates to give ions of *m/z* 193 and 257 corresponding to eliminations of ketene and benzene, respectively (Figure 2b); the formulae of the neutrals were determined by accurate mass measurements of the fragment ions (Table 1). However, the major fragmentation pathway for **4** is the loss of H₂O. The collision energy required for dissociating protonated **4** (relative collision energy 30) is significantly higher than that for the [M + H]⁺ of **1** (relative collision energy 18), the

compound containing a methoxy group at 2-position. The dissociation of the $[M + D]^+$ of **4** occurs with HD scrambling for the expulsions of benzene, the ratio of the abundances for ions of m/z 158 to 157 is 1:1.

Replacing the OCH_3 groups at the 2,2'-positions in compound **1** with OH groups causes the $[M + H]^+$ ion (m/z 267, compound **5**) to dissociate at low collision energy to yield fragment ions of m/z 225 and 173 by eliminations of ketene and phenol (Figure 2c), processes that are analogous to the two fragmentations of compound **1** (Scheme 5). This implies that the CH_3 groups have only a limited role in the fragmentation processes, and by implication, the lone pair of electrons on the oxygen atoms must play a key role in the fragmentation (i.e., facilitating the proton transfers that follow the Nazarov cyclization. In addition, the most abundant fragment is of m/z 147, whereas the corresponding fragment of compound **1** (m/z 171) is not formed, indicating that the acid protons of the phenol rings must play a role in the generation of m/z 147. Furthermore, the formulae of the neutrals lost in the fragmentations were substantiated by accurate mass measurement of the fragment ions.

The dissociations of the $[M-d_2 + D]^+$ ion of m/z 270 were determined by recording the CAD mass spectrum, which reveals that all three fragmentations possible for Compound **5** (Scheme 6) are accompanied by HD scrambling (Figure 3). Eliminations of ketene and ketene-*d* occur with equal probability unlike for $[M+D]^+$ of Compound **1**. The retention of 1, 2, and 3 D occurs during the expulsion of phenol, indicating more extensive HD scrambling, likely due to the labile phenolic protons. The observed HD patterns accompanying the fragmentation processes for these compounds are consistent with the proposed Nazarov cyclization of the original protonated molecules.

Proposed Mechanisms and Theoretical Calculations

We performed theoretical calculations (see Experimental) to aid in the elucidation of the cyclization and fragmentation mechanisms. We addressed cyclization, aryl migration, and subsequent fragmentation of the substituted dibenzalacetone: (**1**) 1,5-bis-(2-methoxyphenyl)-1,4-pentadien-3-one and the cyclization product (**2**) 2,3-bis-(2-methoxyphenyl)-cyclopent-2-ene-1-one. Calculations reveal that the preferred protonation site occurs on the carbonyl oxygen in all cases. We chose the initial forms, **A₁** (Table 2), to be the reference points for calculating relative enthalpies of formation and reaction for all species and reactions (Tables 3, 4, for compound **1** only). In addition to **A₁**, there is an ensemble of other open forms related by rotations about various bonds between the two phenyl rings and the carbonyl group and by means of proton transfer from the carbonyl group. The formation of a protonated cyclization product (**2**) from the initial open protonated precursor (**1**) requires not only a Nazarov condensation but also a migration of the OH group or equivalently the migration of both aryl groups on the ring formed by cyclization. An alternative would be the migration of the protonated carbonyl $C=OH^+$ to an adjacent site prior to Nazarov condensation. We did not discover, however, an energetically feasible route for the migration of the OH moiety either before or after the Nazarov cyclization. We did find, however, that the migration of the aryl groups for the 2-methoxy compound (**1**) (Scheme 7) is facile; analogous routes apply, as determined by DFT calculations, to the unsubstituted compound (**4**), the 2-hydroxy (**5**), the 4-methoxy (**3**), and additionally to the 3-methoxy (**7**) and 3,4-dimethoxy (**6**) analogs; the latter two we did not investigate experimentally (Table 2).

For Compound **1**, the reaction trajectory of $A_{\mathbf{1}} \rightarrow C_{\mathbf{1}} \rightarrow C_{\mathbf{1M}} \rightarrow M_{\mathbf{1}}$, begins with a Nazarov condensation of **A₁** to form a metastable intermediate **C₁** that converts to **C_{1M}**, which is a stable Wagner-Meerwein intermediate stabilized by the 2-methoxy group (Figure 4). From that intermediate, the 1,2-aryl shift occurs and is followed, without any intermediate, by a

second 1,2-aryl shift of the other aryl group thus producing **M₁**, protonated 2,3-*bis*-(2-methoxyphenyl)-cyclopent-4-ene-1-one. The transformation of **A₁** to **M₁** is accomplished with maximum transition-state barrier of 102 kJ/mol, a modest energetic investment.

Similarly, the 4-methoxy (**3**) and the 3,4-dimethoxy (**6**) analogs follow the same trajectory. For both the unsubstituted (**4**) and 3-methoxy (**7**) analogs, which provide little stabilization to the intermediate **C_{1M}** and, surprisingly, also the 2-hydroxy (**5**) form, **C_{1M}** is unstable. Instead, conversions by asynchronous 1,2-aryl Wagner-Meerwein shifts take place directly from **C₁** yielding **M₁** (Scheme 7) and again with modest energetic barriers (Table 2).

The conversion of **M₁** to **M_Z**, protonated 2,3-*bis*-(2-methoxyphenyl)-cyclopent-2-ene-1-one (**2**) from compound **1**, is effected by a series of proton transfers (Scheme 7, Scheme 8a, b). **M_Z** is a very stable form on the potential energy surface at $\Delta^2H_f = -77$ kJ/mol relative to **A₁**. Given that **M_Z** fragments by the same losses in similar proportions to **A₁**, but requiring higher collision energy, the products resulting from ketene and arene (anisole) loss must also be energetically accessible to **M_Z** and likely proceed from a common intermediate along the trajectory from **M₁** to **M_Z**. Given the 1,2-diaryl configuration of **M_Z**, the most direct routes to ketene and arene losses involve the formation of 1,2-diaryl-allyl and protonated 3-aryl-cyclopentadienone cations. But these products (Table S4 in Supplementary Data) require $\Delta^2H_{rxn} = 232$ and 211 kJ/mol, respectively, not including transition state barriers, with respect to **M_Z**. In contrast, formation of 1,3-diaryl-allyl and protonated 3-aryl-cyclopent-4-ene-1-one cations would require 159 and 183 kJ/mol, respectively. Thus, a feasible route to these fragments would require the back migration of the second aryl group as part of the trajectory; these considerations apply to all analogs we explored by DFT calculations. (For fuller discussion of energetically feasible and non-feasible forms, see Table S4 and Schemes S1, S2, S3 in Supplementary Data.)

The conversion of **M₁** to **M_Z** can proceed by direct 1,2-proton migrations over carbon atoms or by aryl-ring assisted or O-facilitated proton transfers (Scheme 8a, b, Table 3, Figure 5). The lowest-energy direct route we discovered is **M₁ → M₆ → M_Z** (Scheme 8a). The first step is proton transfer from C2 to C1, the next step is proton transfer from C3 to C4, followed by spontaneous proton transfer from C1 to C5 forming **M_Z**; the greatest transition state requires 192 kJ/mol relative to **A₁**, yielding a non-competitive route. However, the most energetically favorable route from **M₁** to **M_Z** constitutes an example of intramolecular proton-transport catalysis [35–38], where the mediator is the basic oxygen of the 2-methoxy groups (Scheme 8b). That group is sufficiently basic to abstract protons from the carbon backbone of the five-membered ring. The trajectory for this route is **M₁ → M_{1R} → M_{1X} → M₂ → M_{2R} → M_{2X} → M₃ → M_{3R} → M_Z** in which all proton transfers are to or from a 2-methoxy oxygen coupled with necessary group rotations involving three OH-transfer intermediates; the highest barrier for these processes is 113 kJ/mol (Figure 5). A subroute involves a shunt of trajectory **M_{2R} → M_{2RS} → M_{2RY} → M_Z**; this route has its highest barrier of 119 kJ/mol (Table 3) compared with previous route of 106 kJ/mol and would be competitive starting from **1** but not from **2**. Obviously, the O-assisted routes will not be available for the analogs without a 2-methoxy or 2-hydroxyl moiety, which explains why greater collision energy is required to promote losses of ketene and arene from these protonated ionic species.

Intermediate **M₃** of the proton migration route is the common intermediate from which routes to losses of ketene and arene commence (Scheme 9, Table 4, Figure 6). Of importance is that the distribution of protons on carbons is different than for **C₁** and, hence, the details of aryl migration are different. The trajectory for the common processes is **M₃ → M_{3S} → M_{9S} → M_{9I} → M_{9M}**, where the second arene is transferred from C3 to C4 over a maximum relative barrier of 137 kJ/mol. In the last common intermediate, **M_{9M}**, there is a five-membered ring formed involving C3 and the C2-aryl methoxy oxygen. Cleavage of the

C1–C2 bond followed another C–C cleavage frees nascent ketene for elimination; the trajectory of $\mathbf{M}_{9\mathbf{M}} \rightarrow \mathbf{G}_Z \rightarrow \mathbf{IDC_K} \rightarrow \mathbf{H}_Z + \mathbf{K}$ has a maximum relative barrier of 120 kJ/mol. Starting with $\mathbf{M}_{9\mathbf{M}}$, a series of O-assisted proton transfers and a final C–C bond cleavage frees the arene (anisole) for elimination; trajectory of $\mathbf{M}_{9\mathbf{M}} \rightarrow \mathbf{M}_{10} \rightarrow \mathbf{M}_{10\mathbf{X}} \rightarrow \mathbf{M}_{11} \rightarrow \mathbf{M}_{11\mathbf{X}} \rightarrow \mathbf{IDC_Q} \rightarrow \mathbf{P}_Z + \mathbf{Q}$ has a maximum relative barrier of 113 kJ/mol. The difference in maximum relative enthalpic barrier heights from common $\mathbf{M}_{9\mathbf{M}}$ is in accord with the differences in spectral abundance.

Starting with \mathbf{M}_Z and running back through \mathbf{M}_3 (Scheme 8b) and then through to product \mathbf{H}_Z (Scheme 9), we see that the fate of the charging proton, (indicated by boldface magenta), does not include the adjacent C that is the methylene part of the eliminated ketene. Hence, only ketene, and not *d*-ketene, is eliminated in accord with experiment starting with **2**, and the charging proton ends up on C1 in the product. In addition, the original charging proton from **1** in Scheme 7 and running through Scheme 8b, Scheme 9 is shown in black boldface and indicates possibilities for scrambling: \mathbf{A}_0 interchange with \mathbf{A}_{0k} (Scheme 7) and the back migration of the arene in Scheme 9.

Conclusions

We present here another example of the facility of mass spectrometry to study gas-phase reactions that are models of solution chemistry. The significant similarity in the CAD fragmentations of protonated 1,5-bis-(2-methoxyphenyl)-1,4-pentadien-3-one (**1**) and that of the product of cyclization in the condensed phase, 2,3-diphenylcyclopent-2-ene-1-one (**2**) indicates that Nazarov cyclization occurs in the gas phase as well as in solution and leads to the same product. Moreover, a methoxy or hydroxy group at the 2-position exerts a catalytic effect on the cyclization, rearrangement, and fragmentation series of reactions as seen by the requirement for lower collision energy for the 2-methoxy versus the 4-methoxy isomer and the unsubstituted compound. Theoretical calculations using DFT methods reveal that the basic oxygen of the methoxy group acts as mediator for the various H-migrations following the cyclization. Alternate routes are possible for the unsubstituted and the 4-methoxy analog, but higher energy transition states are required. The application of such gas-phase processes promises to increase the opportunities to use mass spectrometers as preparative devices to synthesize trace amounts of valuable materials and isolate them by soft landing, for example [39, 40].

Supplementary Material

Refer to Web version on PubMed Central for supplementary material.

Acknowledgments

The authors J.C., J.P., and M.G. thank the principal, Sacred Heart College, Thevara, for providing infrastructure. R.S. and V.R. thank Dr. J. S. Yadav, Director, IICT, Hyderabad, for facilities. Research at WU was supported by the National Centers for Research Resources of the NIH, NIGMS grant P41 GM103422-35, and by the Washington University Computational Chemistry Facility, supported by NSF grant CHE-0443501.

References

1. Pellissier H. Recent developments in the Nazarov process. *Tetrahedron*. 2005; 61:6479–6517.
2. Tius M. Some new Nazarov Chemistry. *Eur. J. Org. Chem.* 2005;2193–2206.
3. Frontier AJ, Collison C. The Nazarov cyclization in organic synthesis. Recent advances. *Tetrahedron*. 2005; 61:7577–7606.
4. Yaji K, Shindo M. Construction of a fully substituted cyclopentenone as the core skeleton of stemonamide via a Nazarov cyclization. *Tetrahedron Lett.* 2010; 51:5469–5472.

5. Malona JA, Colbourne JM, Frontier AJ. A general method for the catalytic nazarov cyclization of heteroaromatic compounds. *Org. Lett.* 2006; 8:5661–5664. [PubMed: 17107097]
6. Banaag AR, Tius MA. Design of chiral auxiliaries for the allene ether Nazarov Cyclization. *J. Am. Chem. Soc.* 2007; 129:5328–5329. [PubMed: 17425314]
7. Polo V, Andres J. Lewis acid and substituent effects on the molecular mechanism for the Nazarov reaction of Penta-1,4-dien-3-one and derivatives. A topological analysis based on the combined use of electron localization function and catastrophe theory. *J. Chem. Theory Comput.* 2007; 3:816–823.
8. Smith DA, Ulmer CW. Effects of substituents in the 3-position on the [2 + 2] pentadienyl cation electrocyclization. *J. Org. Chem.* 1997; 62:5110–5115.
9. Shi FQ, Li X, Xia Y, Zhang L, Yu ZX. DFT study of the mechanisms of in water Au(I)-catalyzed tandem [3,3]-rearrangement/Nazarov reaction/[1,2]-hydrogen shift of enynyl acetates: a proton-transport catalysis strategy in the water-catalyzed [1,2]-hydrogen shift. *J. Am. Chem. Soc.* 2007; 129:15503–15513. [PubMed: 18027935]
10. Wang X, Holmes JL. A study of the isomerization and dissociation of formal [acetone-methanol]⁺ ion–molecule complexes. *Can. J. Chem.* 2005; 83:1903–1912.
11. Trikoupis MA, Burgers PC, Ruttink PJA, Terlouw JK. Benzonitrile assisted enolization of the acetone and acetamide radical cations: proton-transport catalysis versus an intermolecular H+/D+ transfer mechanism. *Int. J. Mass Spectrom.* 2001; 210/211:489–502.
12. O'Hair RAJ. The 3D quadrupole ion trap mass spectrometer as a complete chemical laboratory for fundamental gas-phase studies of metal mediated chemistry. *Chem. Commun.* 2006:1469–1481.
13. Kingston EE, Beynon JH, Liehr JG, Meyrant P, Flammang R, Maquestiau A. The Claisen rearrangement of protonated allyl phenyl ether. *Org. Mass Spectrom.* 1985; 20:351–359.
14. Moolayil JT, George M, Srinivas R, Russell A, Giblin D, Gross ML. Protonated nitro group as a gas-phase electrophile: experimental and theoretical study of the cyclization of o-nitrodiphenyl ethers, amines, and sulfides. *J. Am. Soc. Mass Spectrom.* 2007; 18:2204–2217. [PubMed: 17977011]
15. Moolayil JT, George M, Srinivas R, Swamy NS, Russell A, Giblin D, Gross ML. he mass spectrometry-induced cyclization of protonated *N*-[2-(benzoyloxy)phenyl]-benzamide: a gas-phase analog of a solution reaction. *Int. J. Mass Spectrom.* 2006; 249/250:21–30.
16. Zhou Y, Pan Y, Cao X, Wu J, Jiang K. Gas-phase Smiles rearrangement reactions of deprotonated 2-(4,6-dimethoxypyrimidin-2-ylsulfanyl)-*N*-phenylbenzamide and its derivatives in electrospray ionization mass spectrometry. *J. Am. Soc. Mass Spectrom.* 2007; 18:1813–1820. [PubMed: 17719236]
17. Wang F. Collision-induced gas-phase smiles rearrangement in phenoxy-*N*-phenylacetamide derivatives. *Rapid Commun. Mass Spectrom.* 2006; 20:1820–1821. [PubMed: 16676303]
18. Howell JAS, O'early PJ, Yates PC. Acyclic O– and N-substituted pentadienyl cation: structural characterization, cyclisation, and computational results. *Tetrahedron.* 1995; 51(26):7231–7246.
19. Huang J, Leboeuf D, Frontier AJ. Understanding the fate of the oxyallyl cation following Nazarov electrocyclization: sequential Wagner Meerwein migrations and the synthesis of spirocyclic cyclopentenones. *J. Am. Chem. Soc.* 2011; 133:6307–6317. [PubMed: 21466152]
20. George M, Sebastian VS, Nagi Reddy P, Srinivas R, Giblin D, Gross ML. Gas-phase Nazarov cyclization of protonated 2-methoxy and 2-hydroxychalcone: an example of intramolecular proton-transport catalysis. *J. Am. Soc. Mass Spectrom.* 2009; 20:805–818. [PubMed: 19230703]
21. Lawrence NJ, Simon E, Armitage M, Greedy B, Cook D, Ducki S, McGown AT. The synthesis of indanones related to combretastatin A-4 via microwave-assisted Nazarov cyclization of chalcones. *Tetrahedron Lett.* 2006; 47:1637–1640.
22. Adams BK, Ferst EM, Davis MC, Herold M, Kurtkaya S, Camalier RF, Hollingshead MG, Kaur G, Sausville EA, Rickles FR, Snyder JP, Liotta DC, Shojia M. Synthesis and biological evaluation of novel curcumin analogs as anti-cancer and anti-angiogenesis agents. *Bioorg. Med. Chem.* **12**, 3871–3883 (2004). *Tetrahedron Lett.* 2006; 47:1637–1640.
23. Weber WM, Hunsaker LA, Abcouwer SF, Decka LM, Vander Jagt DL. Antioxidant activities of curcumin and related enones. *Bioorganic. Med. Chem.* 2005; 13:3811–3820.

24. Weber WM, Hunsaker LA, Roybal CN, Bobrovnikova-Marjon EV, Abcouwer SF, Royer RE, Decka LM, Vander Jagt DL. Activation of NF κ B is inhibited by curcumin and related enones. *Bioorg. Med. Chem.* 2006; 14:2450–2461. [PubMed: 16338138]
25. Stewart JJP. Optimization of parameters for semiempirical methods. I. Method. *J. Comp. Chem.* 1989; 10:209–220.
26. Stewart JJP. Optimization of parameters for semiempirical methods. II. Applications. *J. Comp. Chem.* 1989; 10:221–264.
27. Frisch, MJ.; Trucks, GW.; Schlegel, HB.; Scuseria, GE.; Robb, MA.; Cheeseman, JR.; Vakrzeswski, VG.; Montgomery, JA., Jr; Stratmann, RE.; Burant, JC.; Dapprich, S.; Millam, JM.; Daniels, AD.; Kudin, KN.; Strain, MC.; Farkas, O.; Tomasi, J.; Barone, V.; Cossi, M.; Cammi, R.; Mennucci, B.; Pomelli, C.; Adamo, C.; Clifford, S.; Ochterski, J.; Petersson, GA.; Ayala, PY.; Cui, Q.; Morokuma, K.; Malick, DK.; Rabuck, AD.; Raghavachari, K.; Foresman, JB.; Cioslowski, J.; Ortiz, JV.; Stefanov, BB.; Liu, G.; Liashenko, A.; Piskorz, P.; Komaromi, I.; Gomperts, R.; Martin, RL.; Fox, DJ.; Keith, T.; Al-Laham, MA.; Peng, CY.; Nanayakkara, A.; Gonzalez, C.; Challacombe, M.; Gill, PMW.; Johnson, B.; Chen, W.; Wong, MW.; Andres, JL.; Gonzalez, C.; Head-Gordon, M.; Replogle, ES.; Pople, JA. Gaussian 98, Revision A.6. Pittsburgh: Gaussian, Inc; 1998.
28. Frisch, MJ.; Trucks, GW.; Schlegel, HB.; Scuseria, GE.; Robb, MA.; Cheeseman, JR.; Montgomery, JA., Jr; Vreven, T.; Kudin, KN.; Burant, JC.; Millam, JM.; Iyengar, SS.; Tomasi, J.; Barone, V.; Mennucci, B.; Cossi, M.; Scalmani, G.; Rega, N.; Petersson, GA.; Nakatsuji, H.; Hada, M.; Ehara, M.; Toyota, K.; Fukuda, R.; Hasegawa, J.; Ishida, M.; Nakajima, T.; Honda, Y.; Kitao, O.; Nakai, H.; Klene, M.; Li, X.; Knox, JE.; Hratchian, HP.; Cross, JB.; Adamo, C.; Jaramillo, J.; Gomperts, R.; Stratmann, RE.; Yazyev, O.; Austin, AJ.; Cammi, R.; Pomelli, C.; Ochterski, JW.; Ayala, PY.; Morokuma, K.; Voth, GA.; Salvador, P.; Dannenberg, JJ.; Zakrzewski, VG.; Dapprich, S.; Daniels, AD.; Strain, MC.; Farkas, O.; Malick, DK.; Rabuck, AD.; Raghavachari, K.; Foresman, JB.; Ortiz, JV.; Cui, Q.; Baboul, AG.; Clifford, S.; Cioslowski, J.; Stefanov, BB.; Liu, G.; Liashenko, A.; Piskorz, P.; Komaromi, I.; Martin, RL.; Fox, DJ.; Keith, T.; Al-Laham, MA.; Peng, CY.; Nanayakkara, A.; Challacombe, M.; Gill, PMW.; Johnson, B.; Chen, W.; Wong, MW.; Gonzalez, C.; Pople, JA. Gaussian 03, Revision C.02. Wallingford CT: Gaussian, Inc; 2004.
29. Frisch, MJ.; Trucks, GW.; Schlegel, HB.; Scuseria, GE.; Robb, MA.; Cheeseman, JR.; Scalmani, G.; Barone, V.; Mennucci, B.; Petersson, GA.; Nakatsuji, H.; Caricato, M.; Li, X.; Hratchian, HP.; Izmaylov, AF.; Bloino, J.; Zheng, G.; Sonnenberg, JL.; Hada, M.; Ehara, M.; Toyota, K.; Fukuda, R.; Hasegawa, J.; Ishida, M.; Nakajima, T.; Honda, Y.; Kitao, O.; Nakai, H.; Vreven, T.; Montgomery, JA., Jr; Peralta, JE.; Ogliaro, F.; Bearpark, M.; Heyd, JJ.; Brothers, E.; Kudin, KN.; Staroverov, VN.; Kobayashi, R.; Normand, J.; Raghavachari, K.; Rendell, A.; Burant, JC.; Iyengar, SS.; Tomasi, J.; Cossi, M.; Rega, N.; Millam, JM.; Klene, M.; Knox, JE.; Cross, JB.; Bakken, V.; Adamo, C.; Jaramillo, J.; Gomperts, R.; Stratmann, RE.; Yazyev, O.; Austin, AJ.; Cammi, R.; Pomelli, C.; Ochterski, JW.; Martin, RL.; Morokuma, K.; Zakrzewski, VG.; Voth, GA.; Salvador, P.; Dannenberg, JJ.; Dapprich, S.; Daniels, AD.; Farkas, O.; Foresman, JB.; Ortiz, JV.; Cioslowski, J.; Fox, DJ. Gaussian 09, Revision A.02. Wallingford CT: Gaussian, Inc; 2009.
30. Zhao Y, Truhlar DG. The M06 suite of density functionals for main-group thermochemistry, thermochemical kinetics, noncovalent interactions, excited states, and transition elements: two new functionals and systematic testing of four M06-class functionals and 12 other functionals. *Theor. Chem. Account.* 2008; 120:215–241.
31. Zhao Y, Truhlar DG. Density functionals with broad applicability in chemistry. *Acct. Chem. Res.* 2008; 41(2):157–167.
32. Scott AP, Radom L. Harmonic Vibrational Frequencies: An Evaluation of Hartree-Fock, MØller-Plesset, Quadratic Configuration Interaction, Density Functional Theory, and Semiempirical Scale Factors. *J. Phys. Chem.* 1996; 100:16502–16513.
33. Shephard MJ, Paddon-Row MN. Gas phase structure of the bicyclo[2.2.1]heptane (norbornane) cation radical: a combined ab initio MO and density functional study. *J. Phys. Chem.* 1995; 99:3101–3108.
34. Turek F. Proton affinity of dimethyl sulfoxide and relative stabilities of C₂H₆OS molecules and C₂H₇OS⁺ ions. A comparative G2(MP2) ab initio and density functional theory study. *Phys. Chem. A.* 1998; 102:4703–4713.

35. Bohme DK. Proton transport in the catalyzed gas-phase isomerization of protonated molecules. *Int. J. Mass Spectrom. Ion Processes.* 1992; 115:95–110.
36. Chalk AJ, Radom L. Proton-transport catalysis: a systematic study of the rearrangement of the isoformyl cation to the formyl cation. *J. Am. Chem. Soc.* 1997; 119:7573–7578.
37. Chalk AJ, Radom L. Ion-transport catalysis: catalyzed isomerizations of NNH^+ and NNCH_3^+ . *J. Am. Chem. Soc.* 1999; 121:1574–1581.
38. Ruttink PJA, Burgers PC, Fell LM, Terlouw JK. Dissociation of Ionized 1,2-Ethanediol and 1,2-Propanediol: Proton-Transport Catalysis with Electron Transfer. *J. Phys. Chem.* 1998; 102:2976–2980.
39. Franchetti V, Solka BH, Baitinger WE, Amy JW, Cooks RG. Soft landing of ions as a means of surface modification. *Int. J. Mass Spectrom. Ion Processes.* 1977; 23:29–35.
40. Verbeck G, Hoffmann W, Walton B. Soft-landing preparative mass spectrometry. *Analyst.* 2012; 137:4393–4407. [PubMed: 22900257]

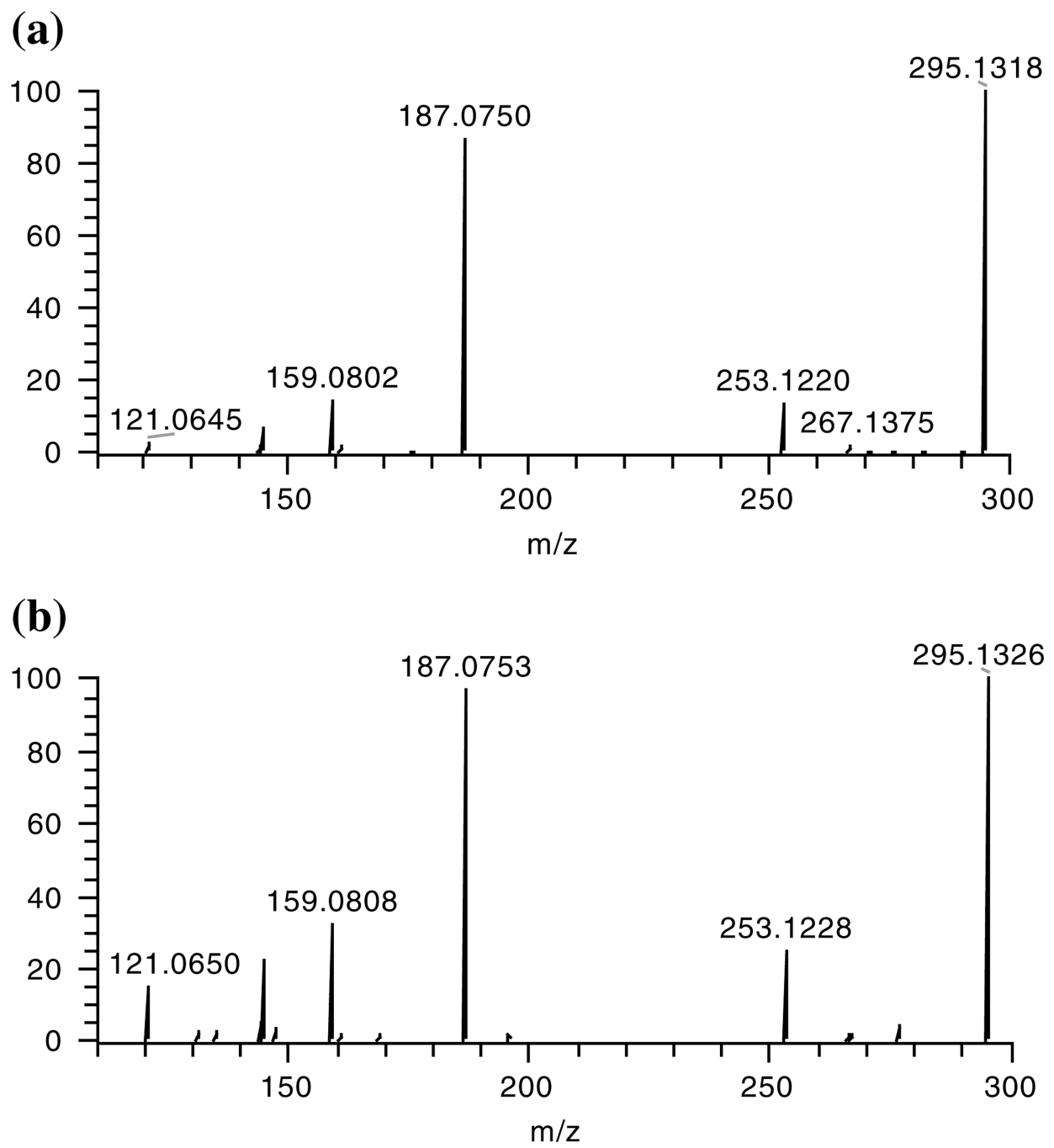
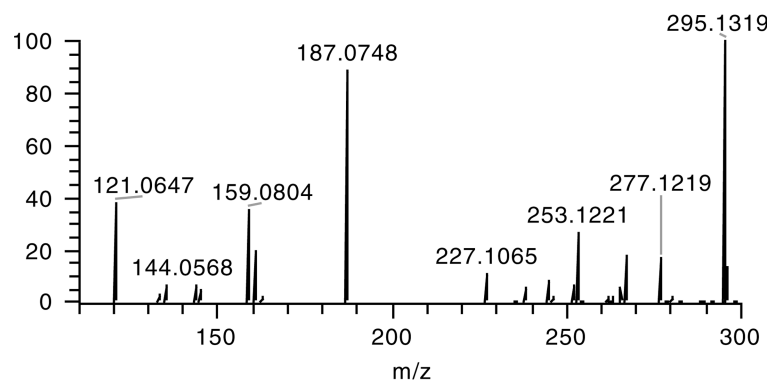


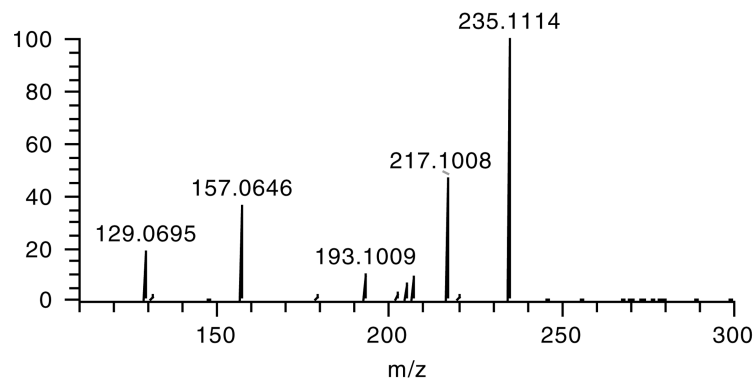
Figure 1.

Positive-ion ESI CAD mass spectra of (a) *bis*-(2-methoxybenzal)acetone (**1**), (b) *2,3-bis*-(2-methoxyphenyl)-cyclopent-2-ene-1-one (**2**): Thermo LTQ Orbitrap mass spectrometer

(a) At collision energy of 30.0



(b) At collision energy of 30.0



(c) At collision energy of 19.0

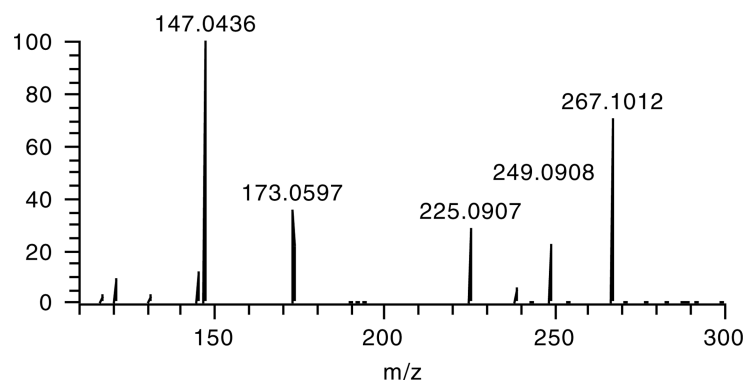


Figure 2.

The CAD mass spectra of the $[M + H]^+$ ions of Compounds (a) 3, (b) 4, and (c) 5; from the Thermo LTQ Orbitrap mass spectrometer

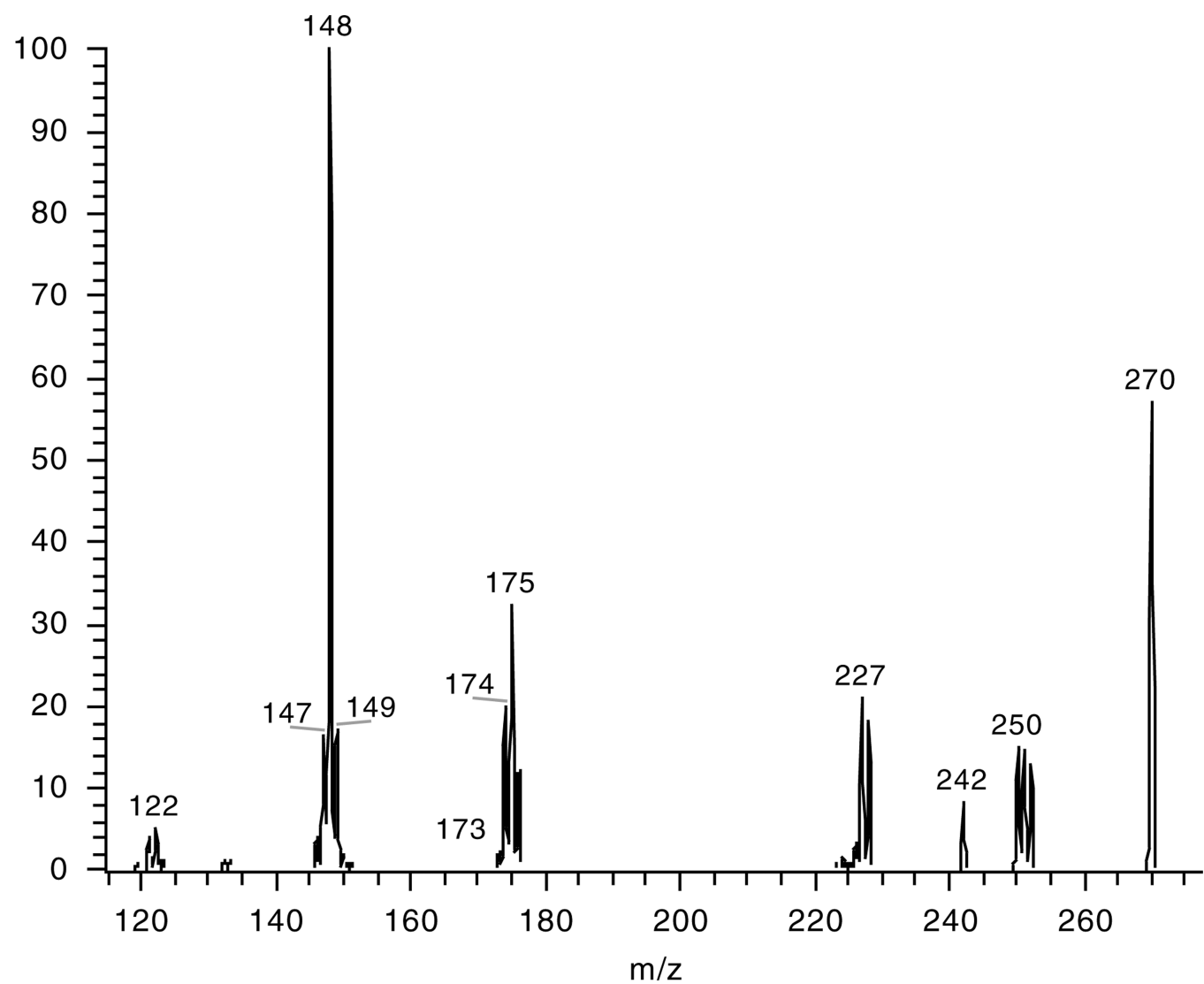
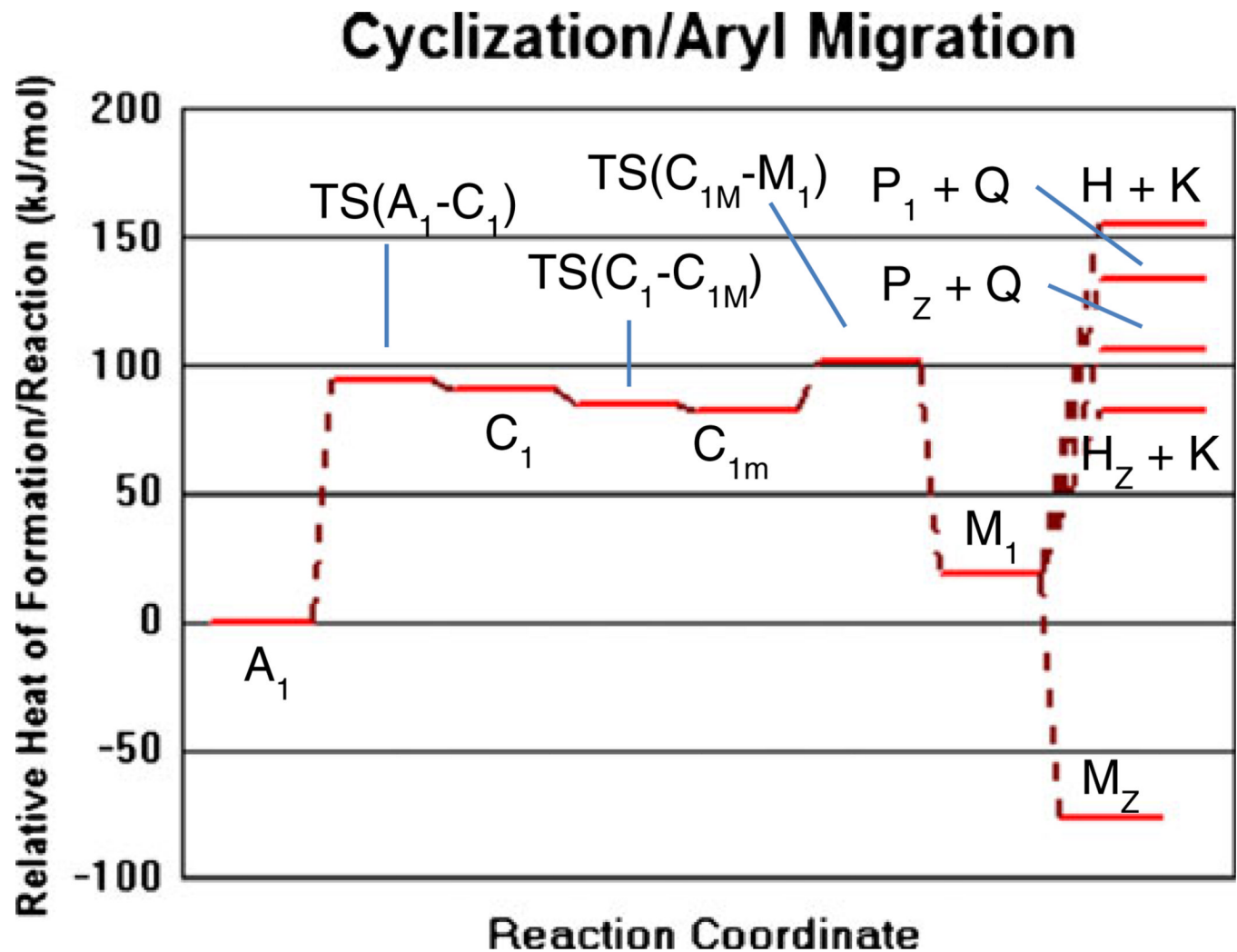
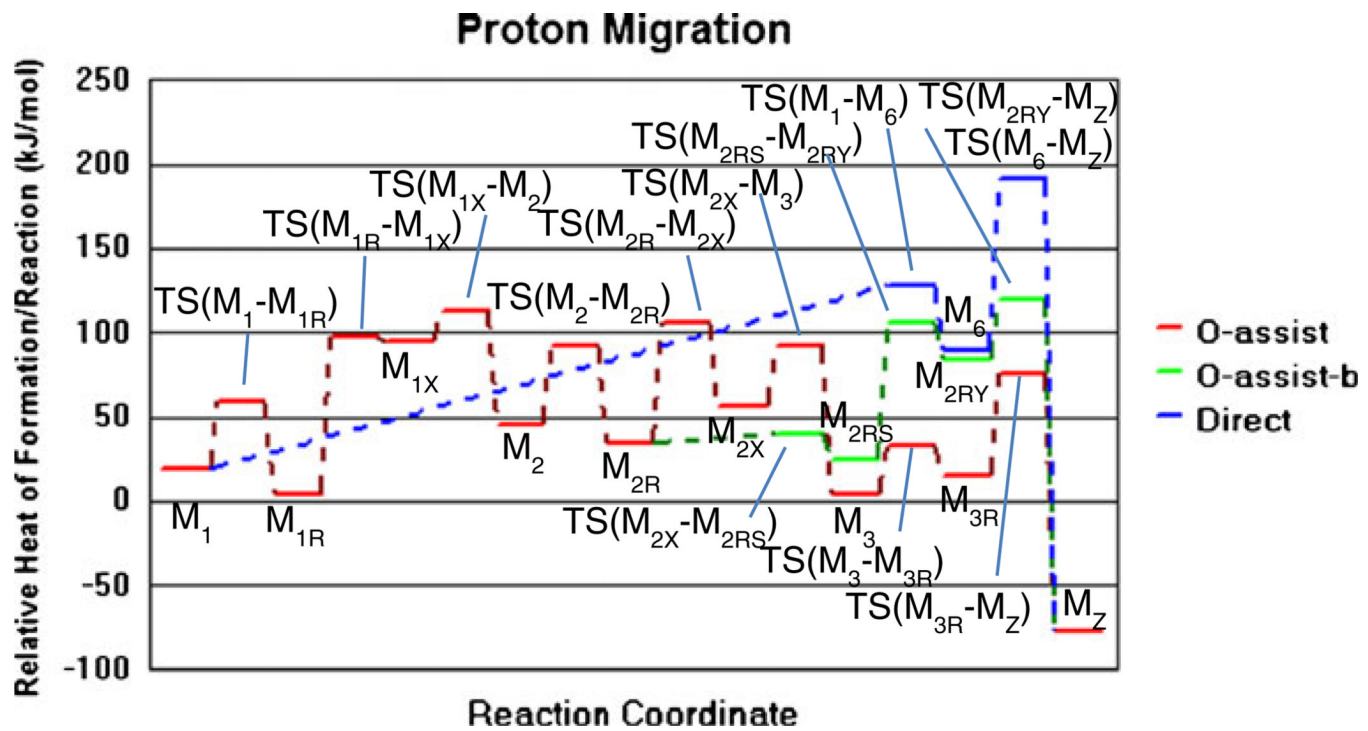


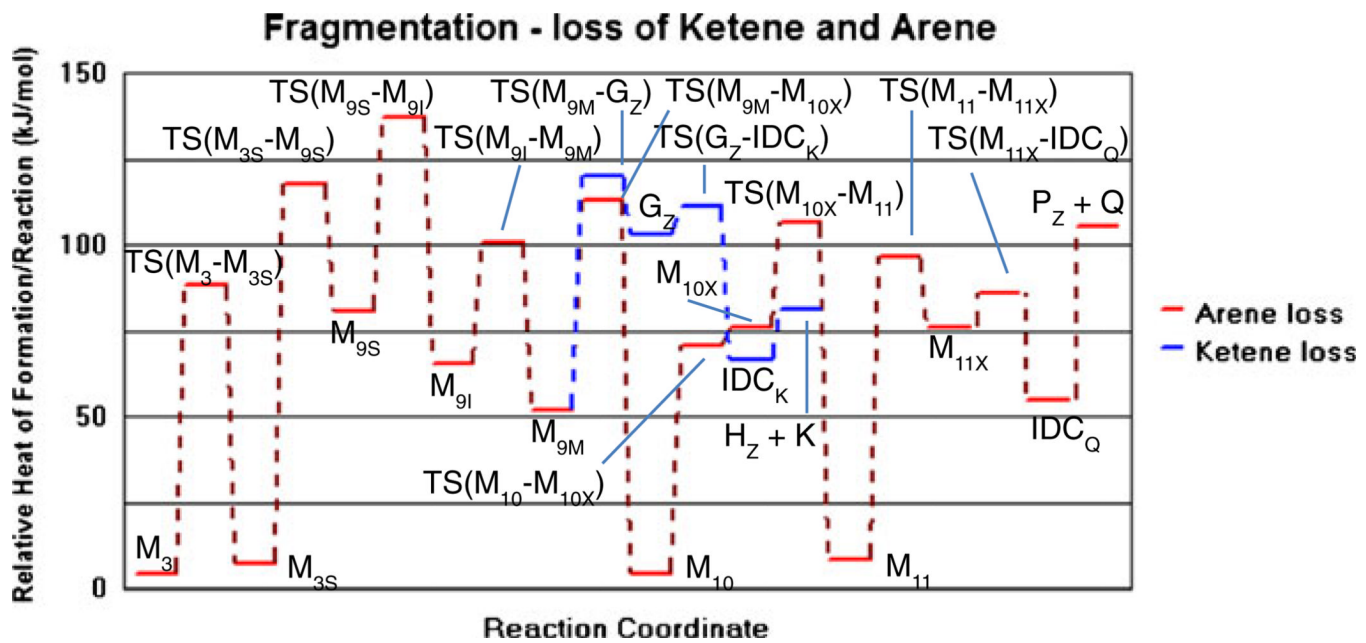
Figure 3.
The CAD mass spectrum of $[M-d_2 + D]^+$ ion generated from **5** by ESI

**Figure 4.**

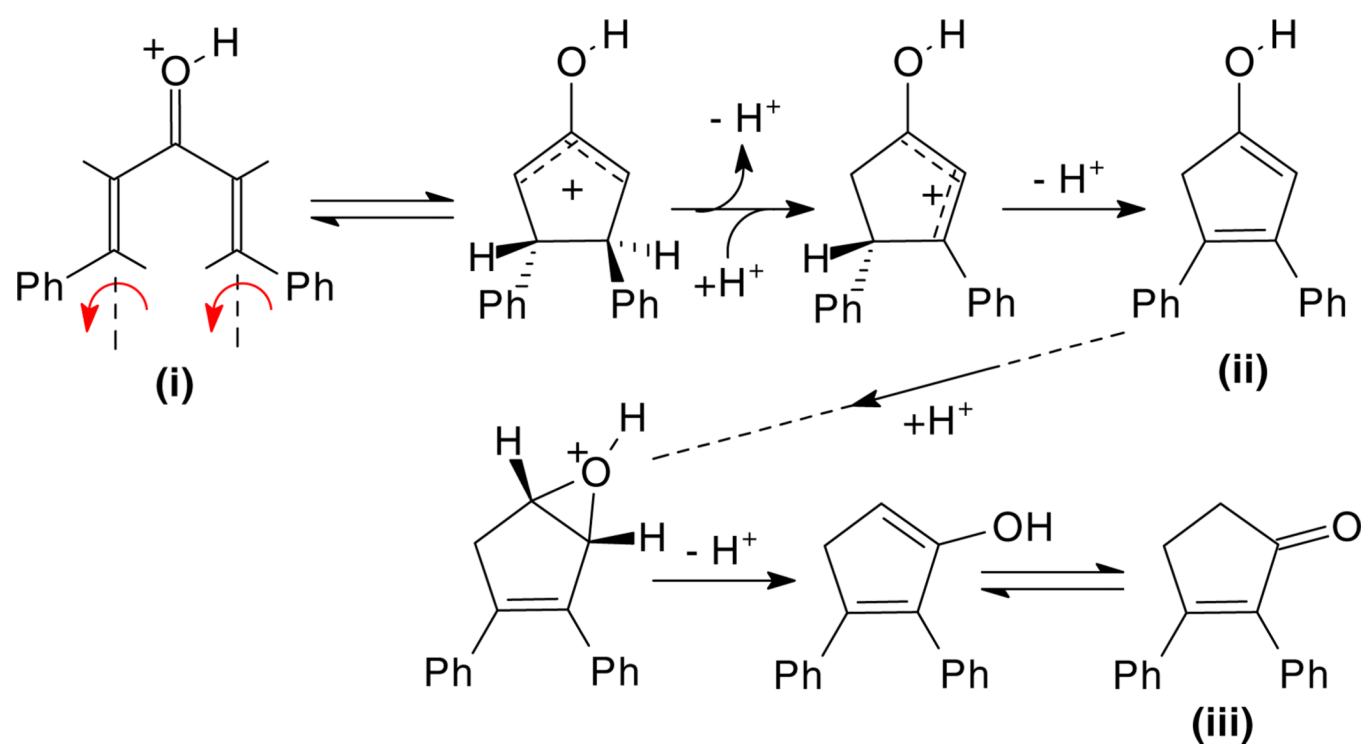
Relative enthalpies of formation/reaction – initial cyclization and aryl migration of o-methoxy Compound (**1**) as example (Scheme 7, Table 2)

**Figure 5.**

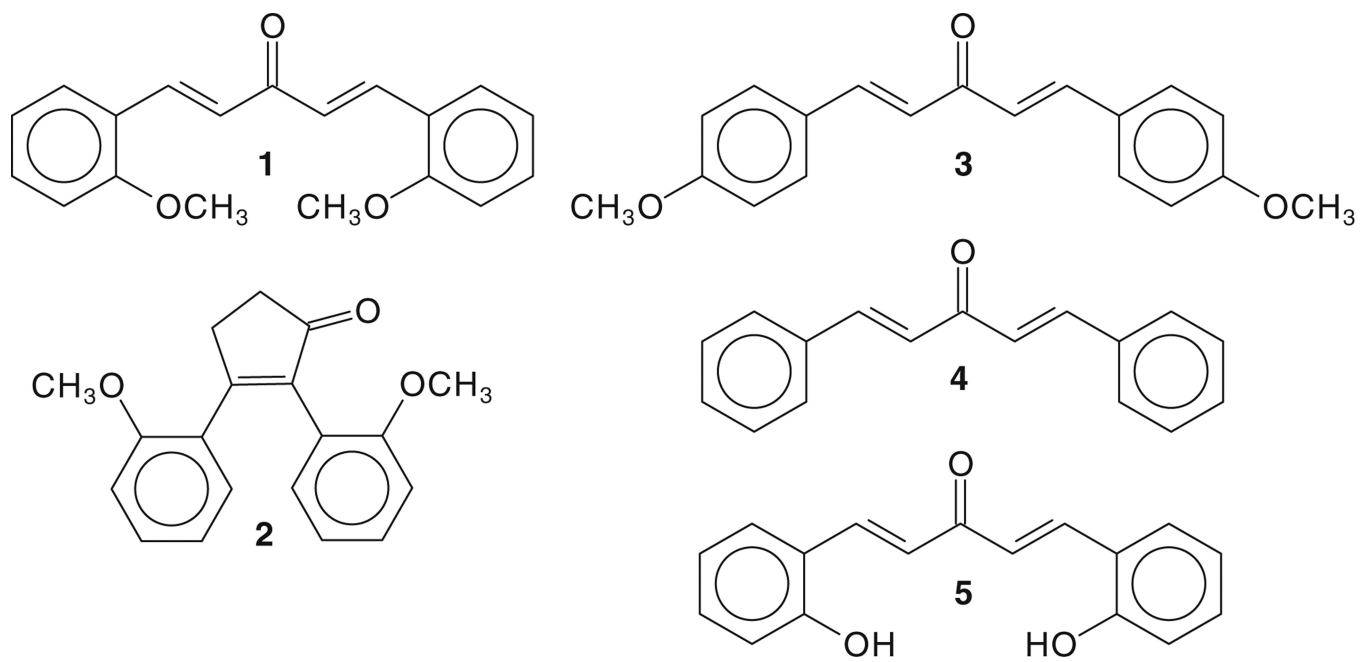
Relative enthalpies of formation/reaction – routes of proton migration in cyclized intermediates from *o*-methoxy Compound (1) (Scheme 8, Table 3)

**Figure 6.**

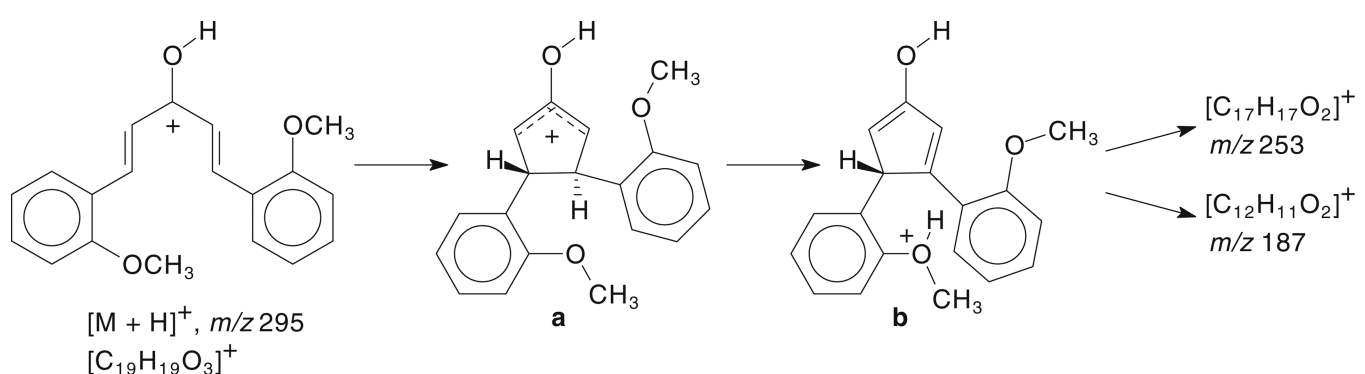
Relative enthalpies of formation/reaction – routes to fragmentation by loss of ketene or arene (*o*-methoxy Compound (1) (Scheme 9, Table 4)



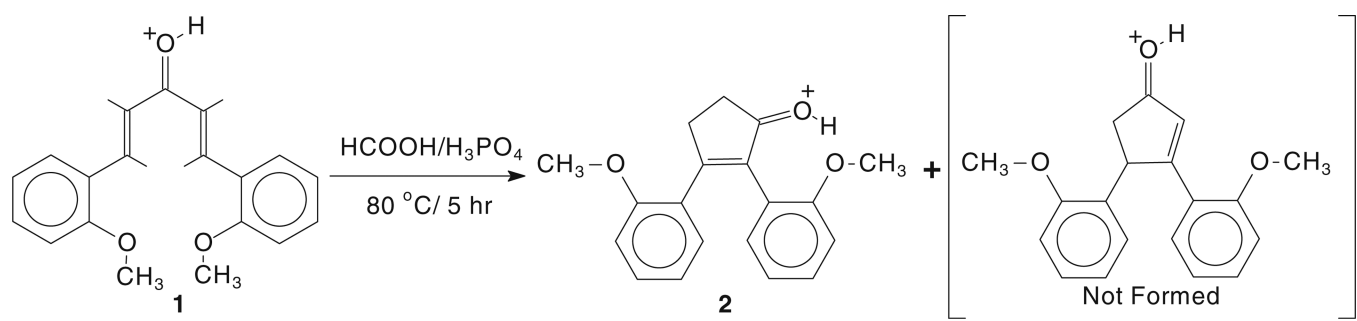
Scheme 1.



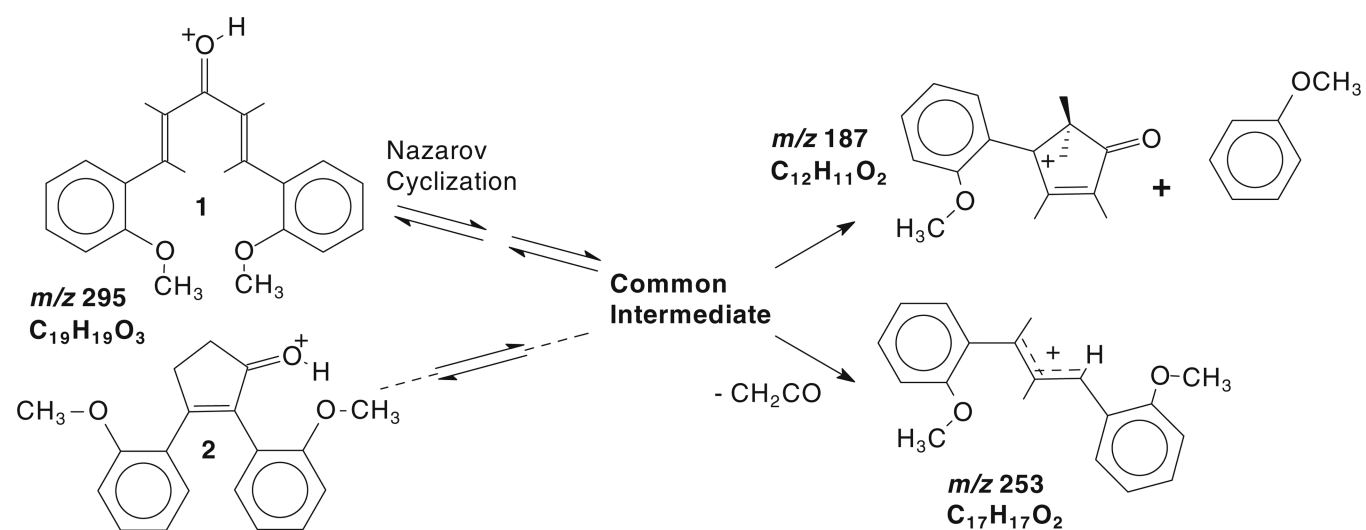
Scheme 2.

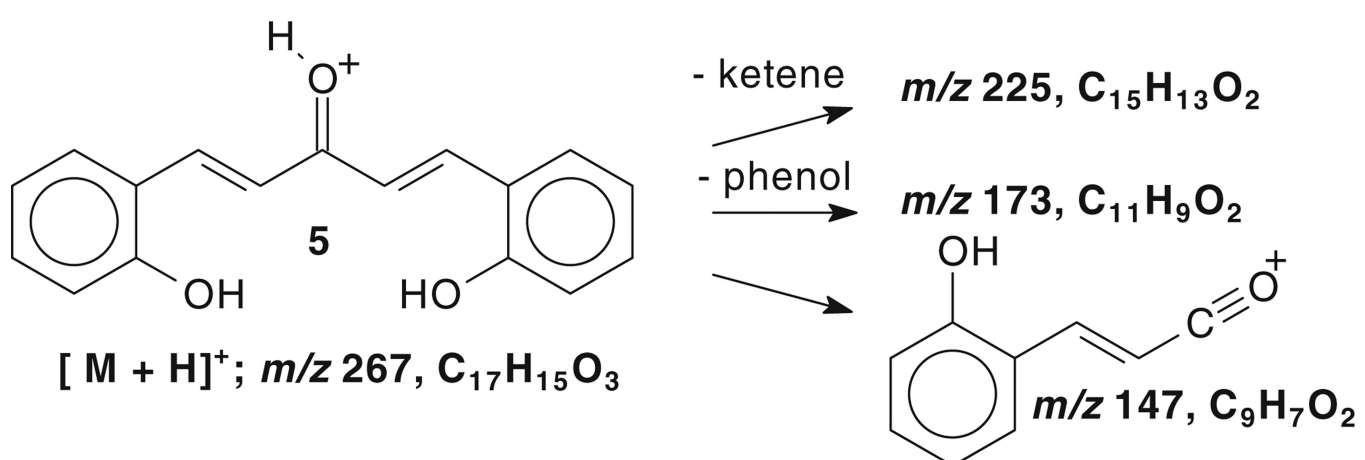


Scheme 3.

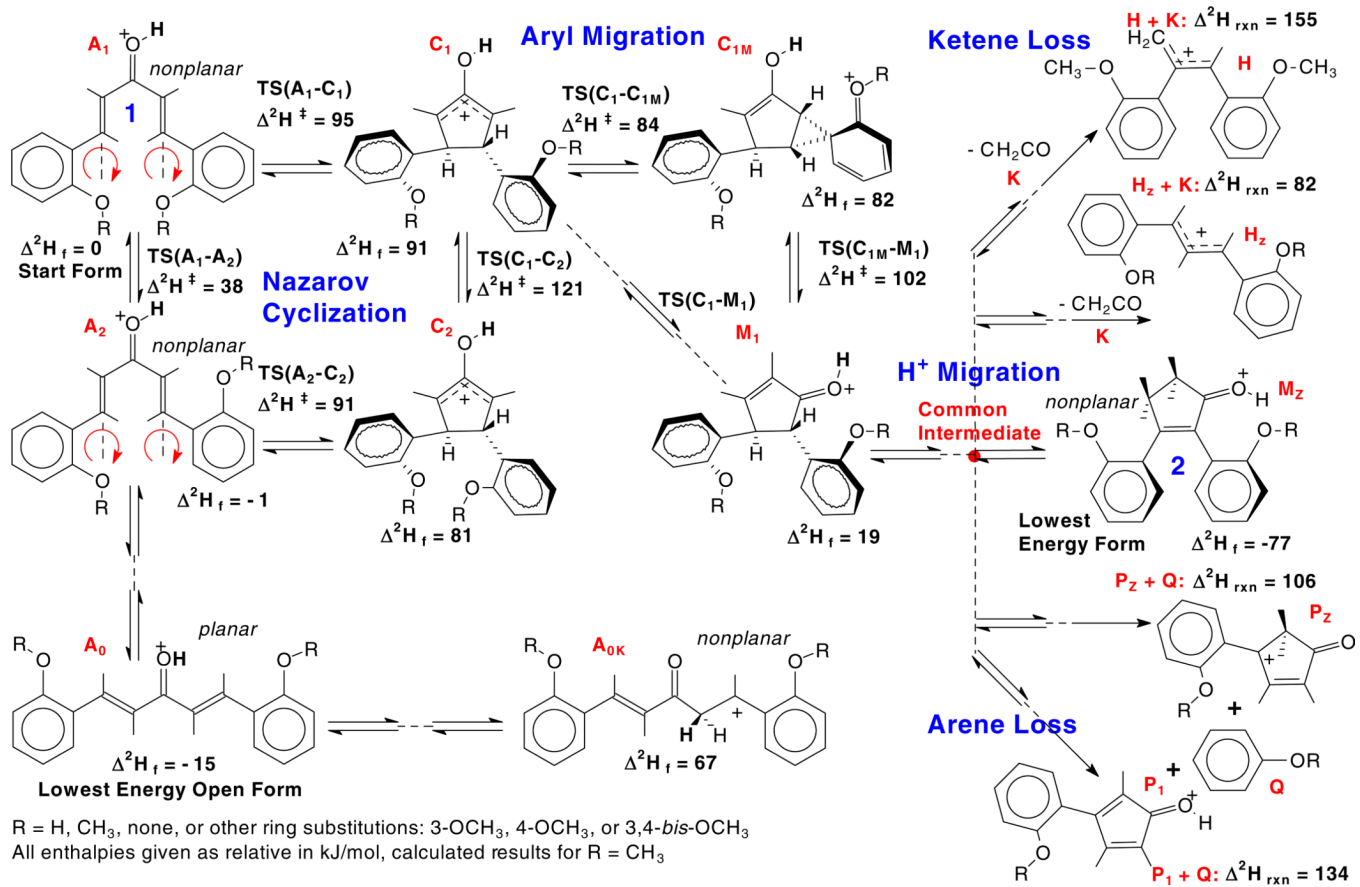


Scheme 4.

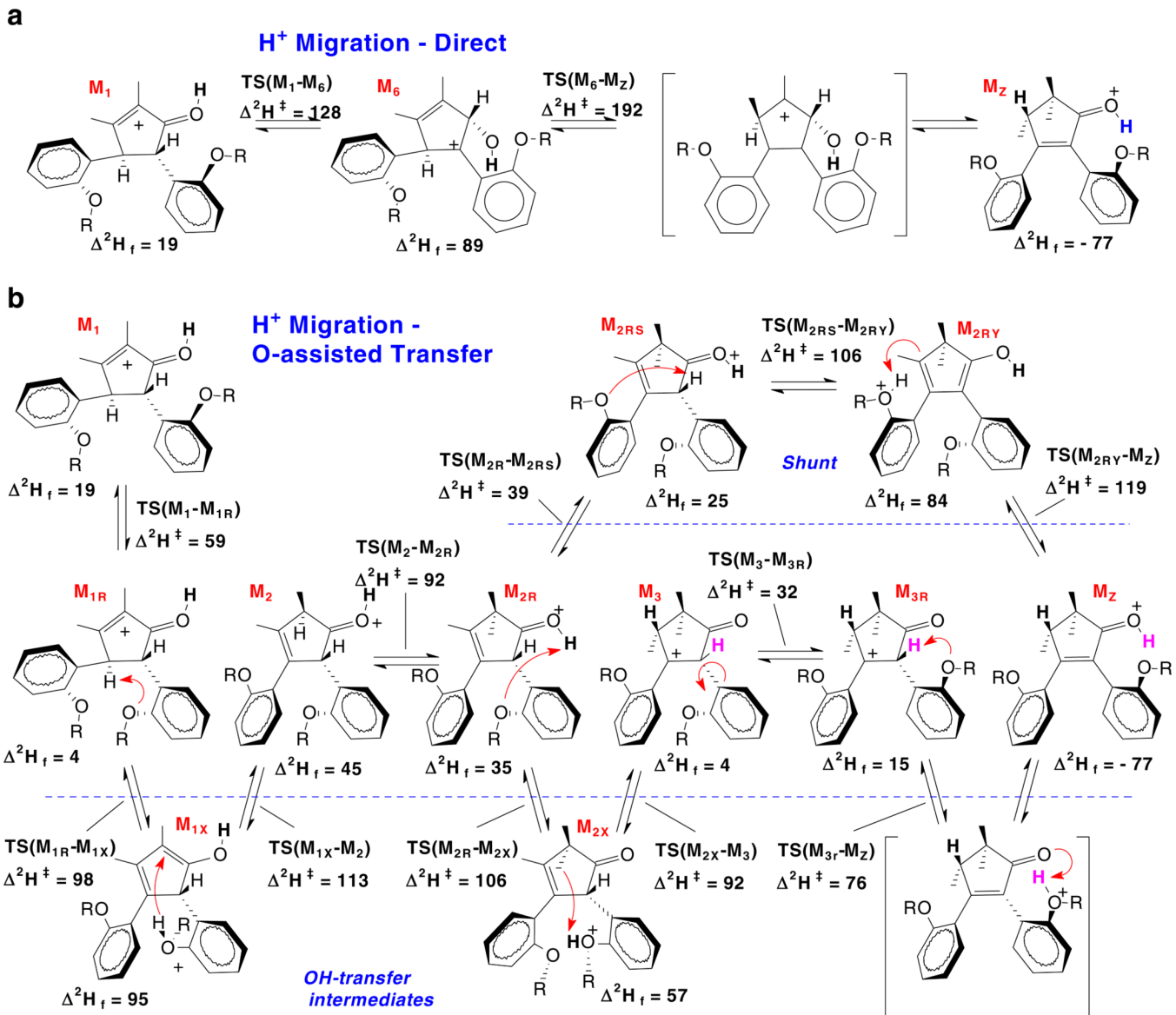




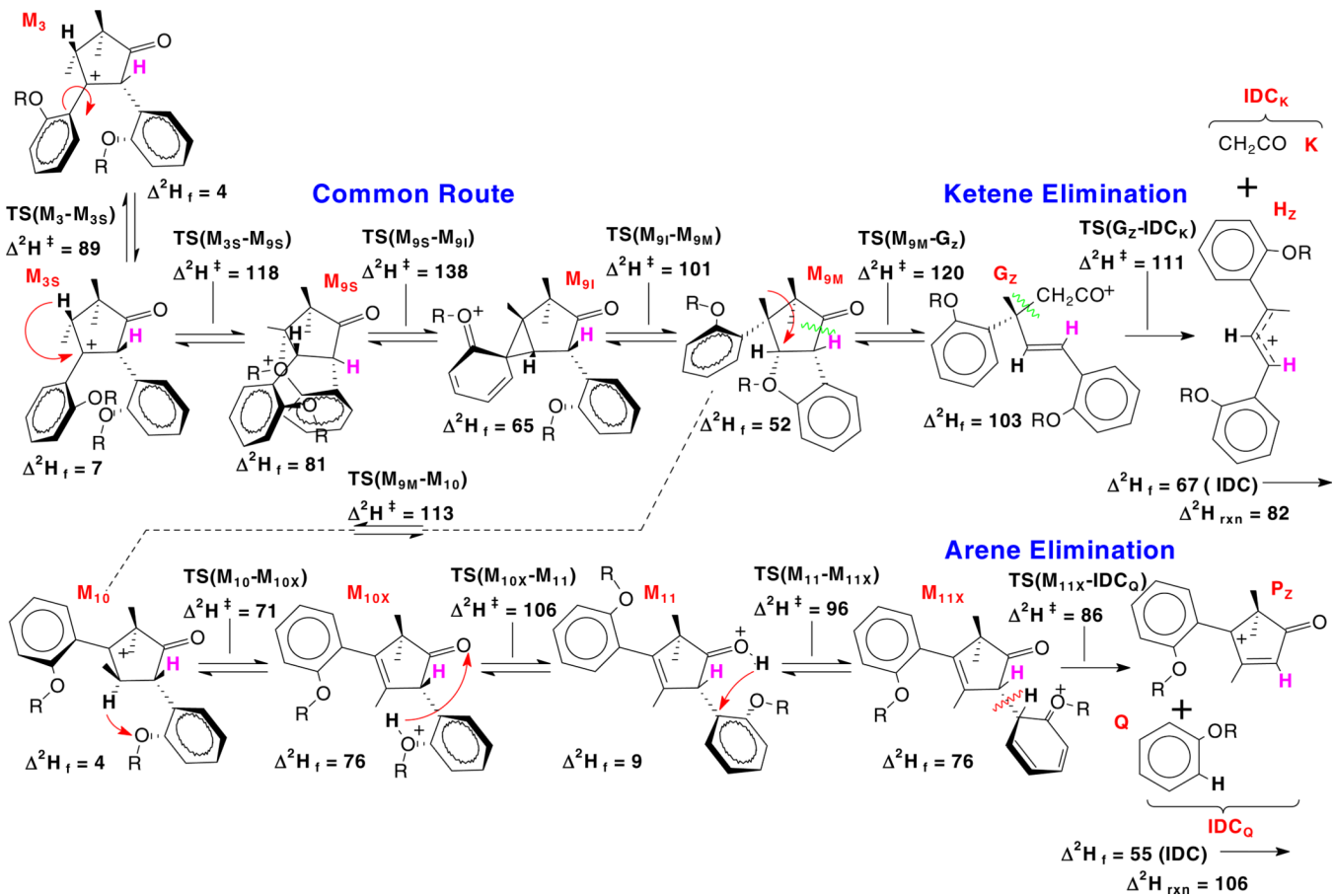
Scheme 6.

**Scheme 7.**

Proposed mechanism for initial cyclization and aryl migration with considerations for proton migration and fragmentation. Enthalpies are given for 2-methoxy(**1**) form, $R = \text{CH}_3$ in kJ/mol

**Scheme 8.**

(a) Proposed mechanisms for proton migrations, 2-methoxy(1) form, R = CH₃. (b) Proposed mechanisms for proton transfers, 2-methoxy(1) form, R = CH₃

**Scheme 9.**

Proposed mechanisms for fragmentation from a common intermediate, 2-methoxy (**1**), R = CH₃

Table 1

Measured Accurate Masses and Elemental Compositions of the $[M + H]^+$ Ions and Major Fragment Ions of Compounds **1–5**

Compound No.	$[M + H]^+$	$[M + H - \text{ketene}]^+$	$[M + H - \text{anisole/C}_6\text{H}_6/\text{phenol}]^+$
1	295.1318	253.1220	187.0750
	$\text{C}_{19}\text{H}_{19}\text{O}_3$	$\text{C}_{17}\text{H}_{17}\text{O}_2$	$\text{C}_{12}\text{H}_{11}\text{O}_2$
	Calc.295.1329	Calc.253.1223	Calc.187.0754
2	295.1326	253.1228	187.0753
	$\text{C}_{19}\text{H}_{19}\text{O}_3$	$\text{C}_{17}\text{H}_{17}\text{O}_2$	$\text{C}_{12}\text{H}_{11}\text{O}_2$
	Calc.295.1329	Calc.253.1223	Calc.187.0754
3	295.1319	253.1221	187.0748
	$\text{C}_{19}\text{H}_{19}\text{O}_3$	$\text{C}_{17}\text{H}_{17}\text{O}_2$	$\text{C}_{12}\text{H}_{11}\text{O}_2$
	Calc.295.1329	Calc.253.1223	Calc.187.0754
4	235.1114	193.1009	157.0646
	$\text{C}_{17}\text{H}_{15}\text{O}$	$\text{C}_{15}\text{H}_{13}$	$\text{C}_{11}\text{H}_9\text{O}$
	Calc.235.1117	Calc.193.1012	Calc.157.0648
5	267.1012	225.0907	173.0597
	$\text{C}_{17}\text{H}_{15}\text{O}_3$	$\text{C}_{15}\text{H}_{13}\text{O}_2$	$\text{C}_{11}\text{H}_9\text{O}_2$
	Calc.267.1016	Calc.225.0910	Calc.173.0597

Calculated Relative Enthalpies of Formation/Reaction (Figure 4, Scheme 7 in kJ/mol)

Cyclization/aryl migration		2-methoxy(1)				2-hydroxy(5)				3-methoxy(7)				3,4-dimethoxy(6)				4-methoxy(3)				
Label	substitution	$\Delta^2\text{H}_f/\Delta^2\text{H}^\ddagger$	$\Delta^2\text{H}_{\text{rxn}}$																			
A ₁		0.0		0.0		0.0		0.0		0.0		0.0		0.0		0.0		0.0		0.0		0.0
TS(A ₁ -C ₁)		94.6		95.5		92.5		105.9		111.3		111.3		95.5								
C ₁		90.7		91.0		83.4		107.2		112.0		112.0		87.9								
TS(C ₁ -M ₁)				105.2		114.3																117.9
TS(C ₁ -C _{1M})				84.1				94.4		108.0												
C _{1M}				82.1				87.7		97.4												
TS(C _{1M} -M ₁)				102.0				106.9		123.6												
M ₁		19.1		18.3		6.5		37.0		40.9		40.9		10.5								
M ₂		-7.0		-78.2		-85.6		-76.6		-72.6		-72.6		-81.3								
H _Z +K				81.8		84.9		90.8		73.7		73.7		74.5								91.5
H+K				154.8		155.5		162.5		150.0		150.0		154.1								164.8
P ₂ +Q				105.7		107.5		104.4		93.6		93.6		95.5								102.9
P ₁ +Q				134.2		133.5		122.4		120.3		120.3		121.3								119.5

Table 3

Calculated Relative Enthalpies of Formation/Reaction (Figure 5, Scheme 8 in kJ/mol)

Proton migration: 2-methoxy(1)		
Label	Corr. H (Hartree)	$\Delta^2H_f/\Delta^2H^\ddagger$ (kJ/mol)
M ₁	-960.085517	19.1
M _{1R}	-960.091319	3.8
M _{1X}	-960.056741	94.6
M ₂	-960.075713	44.8
M _{2R}	-960.079446	35.0
M _{2X}	-960.071093	57.0
M ₃	-960.091108	4.4
M _{3R}	-960.087164	14.8
M _Z	-960.122106	-77.0
M _{2RS}	-960.083390	24.7
M _{2RY}	-960.060868	83.8
M ₆	-960.058937	88.9
TS(M ₁ -M _{1R})	-960.070442	58.7
TS(M _{1R} -M _{1X})	-960.055579	97.7
TS(M _{1X} -M ₂)	-960.049593	113.4
TS(M ₂ -M _{2R})	-960.057758	92.0
TS(M _{2R} -M _{2X})	-960.052313	106.3
TS(M _{2X} -M ₃)	-960.057718	92.1
TS(M ₃ -M _{3R})	-960.080465	32.3
TS(M _{3R} -M _Z)	-960.063781	76.1
TS(M _{2R} -M _{2RS})	-960.077833	39.3
TS(M _{2RS} -M _{2RY})	-960.052436	105.9
TS(M _{2RY} -M _Z)	-960.047349	119.3
TS(M ₁ -M ₆)	-960.044170	127.6
TS(M ₆ -M _Z)U	-960.013145	209.1
TS(M ₆ -M _Z)L	-960.019680	191.9

Table 4

Calculated Relative Enthalpies of Formation/Reaction (Figure 6, Scheme 9 in kJ/mol)

Fragmentation - loss of ketene/arene:			
Label	Corr. H (Hartree)	$\Delta^2H_f/\Delta^2H^\ddagger$ (kJ/mol)	Δ^2H_{rxn} (kJ/mol)
M ₃	-960.091108	4.4	
M _{3S}	-960.090036	7.2	
M _{9S}	-960.062019	80.8	
M _{9I}	-960.067870	65.4	
M _{9M}	-960.073040	51.8	
G _Z	-960.053562	103.0	
IDC _K	-960.067245	67.1	
H _Z	-807.540968		81.8
K	-152.520672		
M ₁₀	-960.091171	4.2	
M _{10X}	-960.063801	76.1	
M ₁₁	-960.089460	8.7	
M _{11X}	-960.063719	76.3	
IDC _Q	-960.071879	54.9	
P _Z	-613.578823		105.7
Q	-346.474167		
TS(M ₃ -M _{3S})	-960.059049	88.6	
TS(M _{3S} -M _{9S})	-960.047967	117.7	
TS(M _{9S} -M _{9I})	-960.040415	137.5	
TS(M _{9I} -M _{9M})	-960.054346	100.9	
TS(M _{9M} -M ₁₀)	-960.049736	113.0	
TS(M ₁₀ -M _{10X})	-960.065835	70.8	
TS(M _{10X} -M ₁₁)	-960.052227	106.5	
TS(M ₁₁ -M _{11X})	-960.056033	96.5	
TS(M _{11X} -IDC _Q)	-960.059922	86.3	
TS(M _{9M} -G _Z)	-960.046945	120.3	
TS(G _Z -IDC _K)	-960.050375	111.3	